

Materials Map Integrating Experimental and Computational Data through Graph-Based Machine Learning for Enhanced Materials Discovery

Yusuke Hashimoto and Takaaki Tomai

Frontier Research Institute for Interdisciplinary Sciences, Tohoku University, Sendai, Japan, 980-8577

Xue Jia and Hao Li

Advanced Institute for Materials Research (WPI-AIMR), Tohoku University, Sendai, Japan, 980-8577

(Dated: March 12, 2025)

Materials informatics (MI), which emerges from the integration of materials science and data science, is expected to greatly streamline the material discovery and development. The data used for MI are obtained from both computational and experimental studies, while their integration remains challenging. In our previous study, we reported the integration of these datasets by applying a machine learning model that captures trends hidden in the experimental datasets to compositional data stored in the computational database. In this study, we use the obtained data to construct materials maps, which visualize the relation in the structural features of materials, aiming to support study by the experimental researchers. The map is constructed using the MatDeepLearn (MDL) framework, which implements the graph-based representation of material structures, deep learning, and dimensional reduction for the map construction. We evaluate the obtained materials maps through statistical analysis and found that the MDL using message passing neural network (MPNN) enables efficient extraction of features that reflect the structural complexity of materials. Moreover, we found that this advantage does not necessarily translate into improved accuracy in predicting material properties. We attribute this unexpected outcome to the high learning performance inherent in MPNN, which can contribute to the structuring of data points within the materials map.

I. INTRODUCTION

Materials informatics has emerged as a transformative approach to accelerate materials development by integrating data science with materials science [1–5]. Through the application of artificial intelligence (AI) and machine learning (ML), researchers can efficiently identify and design materials with desired properties, significantly reducing the time and cost associated with traditional experimental methods. The success of such approaches relies heavily on the availability of high-quality, large-scale datasets. Initiatives such as the Materials Project (MP) [6] and AFLOW [7] have been instrumental in systematically collecting and organizing results from first-principles calculations conducted globally. These databases, when combined with advanced data science techniques, enable the development of machine learning models capable of predicting material properties with remarkable accuracy [8]. A critical challenge persists in bridging the gap between theoretical predictions and practical applications. While computational databases provide extensive datasets derived from first-principles calculations, experimental data remains sparse, inconsistent, and often lacks the structural information necessary for advanced modeling. This disparity between computational and experimental data presents a significant obstacle to the full realization of materials informatics potential.

When traveling to a destination, we often refer to maps to find directions. In contrast, materials development often relies heavily on trial and error guided by experience and intuition, which can result in low efficiency. If materials maps that provide guidance for investigation were

built, we could potentially achieve more efficient materials development. Recently, researches on creating materials maps using data science-based approaches, such as t-SNE (t-distributed stochastic neighbor embedding) [9–15] and UMAP (Uniform Manifold Approximation and Projection) [16–19], have been actively pursued in the field of materials science.

In general, materials are described by their atomic compositions; however, their properties are fundamentally determined by not only atomic composition but also structural arrangement. To address the limitations of simple chemical formulas in capturing structural nuances, researchers have developed graph-based approaches. The Crystal Graph Convolutional Neural Network (CGCNN) [20] models materials as graphs, where nodes correspond to atoms and edges represent interactions. This method encodes structural information into high-dimensional feature vectors, which, when combined with deep learning techniques, enable the development of robust property prediction models [8].

The implementation of graph-based representations and property prediction models requires advanced computational tools. MatDeepLearn (MDL) [8], developed by Fung et al., provides an efficient Python-based environment for developing material property models. MDL supports various models, including CGCNN [20], Message Passing Neural Networks (MPNN) [21], MatErials Graph Network (MEGNet) [22], SchNet [23], and Graph Convolutional Networks (GCN). The open-source nature and extensibility of MDL make it valuable for researchers implementing graph-based materials property predictions by deep-learning based architectures [8].

The application of graph-based representation mate-

materials properties relies heavily on structural data availability [20]. While first-principles calculations inherently include structural information, experimental datasets often lack such details. This limitation poses challenges for applying graph-based methods to experimental data, causing most studies that employ graph-based representations of material properties to rely primarily on computational datasets [8].

StarryData2 (SD2) is an innovative database project in the field of materials science [24]. Developed by Katsura *et al.*, this database aims to systematically collect, organize, and publish experimental data on materials from previously published papers. SD2 has extracted information from over 7,000 papers, including thermoelectric property data for more than 40,000 samples. The database covers a wide range of material fields, including thermoelectric materials, magnetic materials, low thermal conductivity materials, aggregates, high thermal conductivity materials, and piezoelectric materials. Designed for open access, SD2 allows researchers and engineers to freely access and utilize the data.

In our previous study [25], we proposed a novel framework to integrate experimental and computational datasets to create a comprehensive data for materials informatics. As briefly described in SI, our approach consisted of the following steps: preprocessing experimental data, training a machine learning model, and applying the trained model to predict experimental data for the compositions registered in the computational data. As a result, we obtained a dataset of the predicted experimental values of material properties (zT) with structural information of the corresponding materials.

In this study, we use this dataset to construct material maps with MDL. The creation of interpretable material maps that reflect real-world variability provides a novel framework for efficient material discovery. The contributions of this study are summarized as follows:

- We construct materials maps reflecting the relation between the predicted experimental values of thermoelectric properties (zT values) and the corresponding material structures.
- We demonstrate the effectiveness of the MPNN architecture [21] in capturing structural complexity of materials.
- We provide a systematic analysis of structures in obtained material maps with respect to the graph-based model used in MDL and its hyperparameters.
- We highlight the potential of material maps as a tool for guiding experimentalists in synthesizing new materials, enabling efficient exploration of materials design spaces.

II. METHOD

As schematically described in Figure 1, we here construct materials maps by MDL, which implements graph-based representation of materials properties, deep learning, and dimensional reduction by the t-SNE algorithm [8]. We use the dataset extracted by our previous study, described in Ref. [25] and briefly summarized in SI. This dataset comprises over 1,000 materials, each represented by its structural information and predicted experimental zT values. The structural information includes atomic positions and lattice parameters, enabling the construction of graph-based representation of materials by MDL [8], which provides a flexible environment for material property prediction. As schematically described in Figure 1, the model defined in MDL is composed of input, embedding, graph convolution, pooling, dense, and output layers. The entire model is trained using material structures as input and the corresponding predicted zT values as output. The input layer primarily extracts basic structural information, such as atomic positions, types, and bond distances, using the Atomic Simulation Environment (ASE) framework. The obtained data serves as the foundation for constructing graph structures and developing advanced machine learning models, including deep learning approaches. MDL supports the construction of material maps using t-SNE with the data from the first dense layer, which is placed after GC layer as schematically described in Figure 2. This configuration allows the model to capture both local and long-range structural correlations learned by the GC layer.

In this study, we mainly discuss materials maps generated using MPNN [21], which produces well-structured materials map efficiently. In MDL, MPNN is characterized by the Graph Convolutional (GC) layer configured by the neural network (NN) layer and the gated recurrent unit (GRU) layer. The NN layer enhances the model’s representational capacity, while the GRU layer improves learning efficiency through memory mechanisms. The number of GC layer repetitions was set to 4, which is the default hyperparameter [8] of MDL, unless otherwise specified.

III. RESULTS

A. Material Map Generated Using MPNN Architecture

Let us first demonstrate a material map generated using the MPNN [21] architecture in Figure 2. The default hyperparameters of MDL [8] were used in the model training. The x and y axes represent the first and second t-SNE components, while the color of each point represents the predicted experimental zT value. In the figure, we find a clear trend where lower zT values concentrate in the lower region, while higher values appear in the upper region. The smooth color gradients reflect meaningful

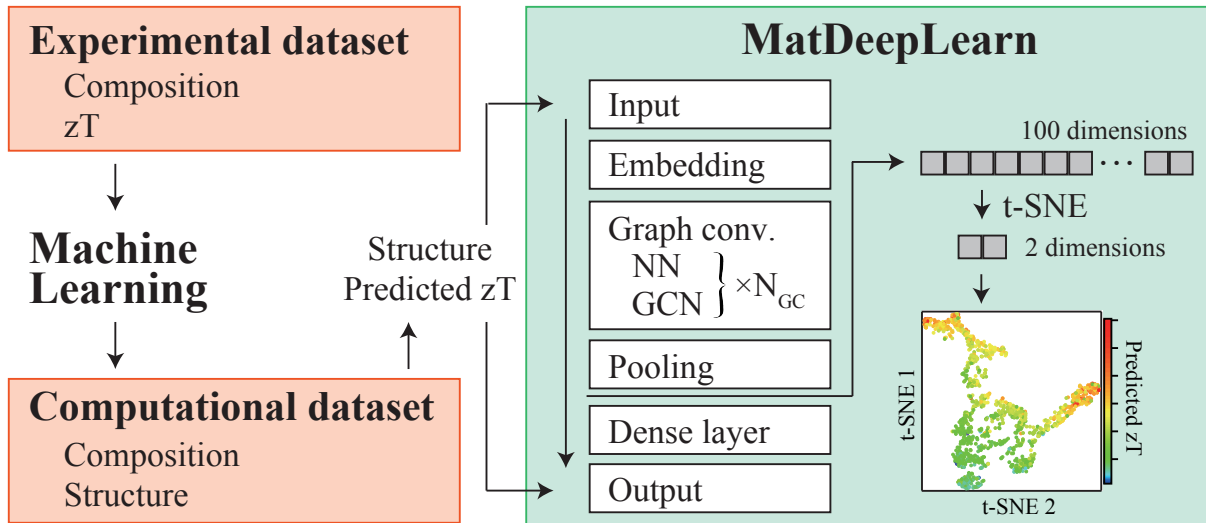


FIG. 1. Schematic representation of the data flow and data analysis processes employed in this study.

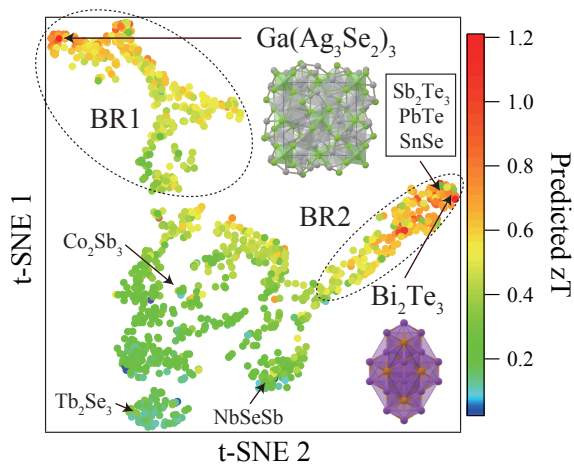


FIG. 2. A materials map generated by MDL using MPNN architecture for graph-based modeling of materials properties. The color of each data point represents the predicted-experimental zT values. The position of each data point is extracted by the model implemented in MDL. Two branches spreading laterally are labeled BR1 and BR2 in the map. The structures of Bi_2Te_3 and $\text{Ga}(\text{Ag}_3\text{Se}_2)_3$ are demonstrated to illustrate the different complexities among the materials included in the two branches.

relationships between predicted zT values and structural features. We also find two distinct branches, labeled BR1 and BR2 in Figure 2, extended laterally in the upper portion, featuring significant clusters of high zT values at

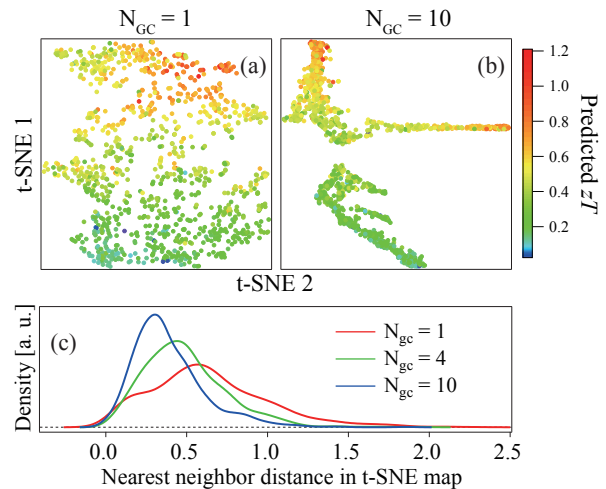


FIG. 3. Comparison of the material maps generated by MDL with (a) one GC layer ($N_{GC} = 1$), and (b) ten GC layers ($N_{GC} = 10$). (c) The structures in the maps for $N_{GC} = 1, 4$, and 10 are compared by the distribution analysis of NND for each data point by KDE.

their endpoints. The fine structures visible in the map suggest that the model effectively captures structural features of materials.

B. Contribution of GC Layer in MPNN Architecture for Map Construction

In MDL, the graph-based architecture is implemented in the GC layer, characterized by GC type, GC dimensions, and the repetition number of GC blocks (N_{GC}). To investigate the role of the GC layer, we compare the maps generated by MDL with $N_{GC} = 1$ and 10 in Figure 3. We find that the increase in N_{GC} leads to tighter clustering of data points. To quantify the structures in the map, we evaluate the distributions of the nearest neighbor distances (NND) of each data point by Kernel Density Estimation (KDE) [26]. KDE is a non-parametric method for estimating smooth probability density functions from data points, and thus offers a more continuous and less biased distribution representation than histograms. Figure 3(c) summarizes the KDE spectra obtained with $N_{GC} = 1, 4$ (default value for MDL), and 10. With increasing N_{GC} , the peak intensity increases and the peak position shifts to the lower NND region, convincing the enhanced feature learning by the GC layer.

The framework of DeeperGATGNN allows machine learning modeling with large N_{GC} [15]. With increasing N_{GC} , prediction accuracy and structural feature learning are enhanced, while memory usage for computation increases dramatically especially when large datasets are used for the analysis [15]. Therefore, the use of MDL with MPNN architecture may be limited to cases where the dataset size is relatively small or when computing resources with sufficient memory size are available.

In MDL, the MPNN architecture is characterized by NN and GRU blocks in the GC layer. To investigate the contributions of each block, we selectively controlled the training of each block, turning them ON or OFF, by modifying the MDL code. N_{GC} was again set to 10 to enhance the contribution of each block. Figures 4(a)-4(d) illustrate the effects of disabling learning in either the NN or GRU blocks. When learning is disabled in either block, the points spread more diffusely; when both are disabled, the points distribute uniformly across the map. These trends are again clearly captured by the results of KDE, shown in Figure 4(e), as the increase in the peak intensity and the peak shift toward the lower NND region by turning ON the training by either or both of the NN and GRU blocks. Overall, these results demonstrate that learning by the GC layer, composed of the NN and GRU blocks, plays a crucial role the structural organization in the materials map.

C. Model Dependency of Material Maps

So far, we have discussed material maps generated by MDL using the MPNN architecture. MDL also supports other architectures, which are highly sophisticated and specialized for analyzing material properties, such as CGCNN [20], MEGNet [22], GCN, and SchNet [21]. In Figures 5(a)-5(d), we compare the material maps gen-

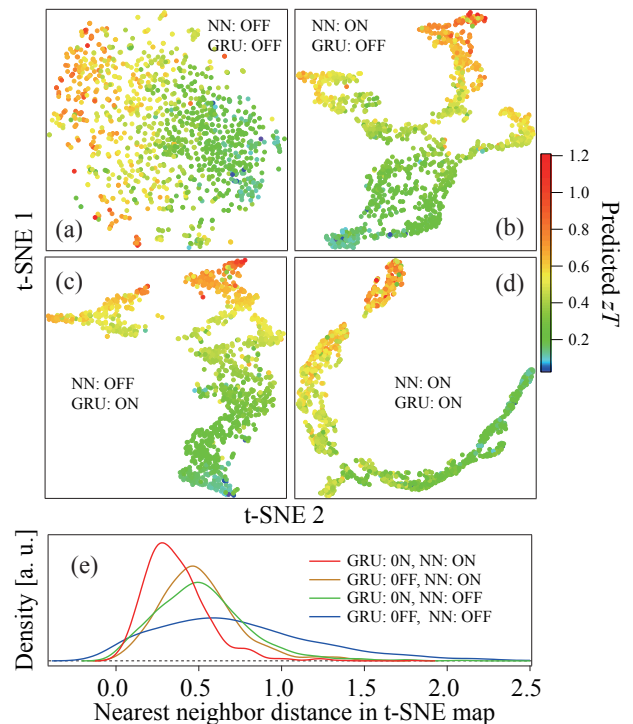


FIG. 4. Materials maps generated by MDL with different training configurations in the GC layer, composed of neural networks (NN) and gated recurrent units (GRU). To emphasize the contribution of the GC layers, $N_{GC} = 10$ was selected. The training for each units are separately controlled as (a) NN: OFF, GRU: OFF, (b) NN: ON, GRU: OFF, (c) NN: OFF, GRU: ON, and (d) NN: ON, GRU: ON. Each map illustrates how the configurations of GC layer influence the distribution of data points in the materials map. The structures in the maps shown in (a)-(d) are compared by the distribution analysis of NND of each data point by KDE.

erated by each of these models and find that the maps generated by the other models lack the clear structures observed in the map generated by MPNN. These trends are again evaluated by the distribution analysis of NND of each data point by KDE, as summarized in Figure 5(e). We find that the KDE spectrum for the MPNN-generated map displays a higher density in the low NND region compared to the spectra for other models. These trends are emphasized by increasing the repetition number the GC layer, leading us to convince the superiority of MPNN as an effective tool providing more structurally organized and continuous mappings compared to other graph-based models.

Similar discussions are found in Ref. [8], which is the first report of MDL. This study also compares material maps generated with different models; however, the differences in the obtained maps were not as significant compared to the present case. We attribute the difference in these two studies to the data screening applied in our study. Both studies use the same database, Materials

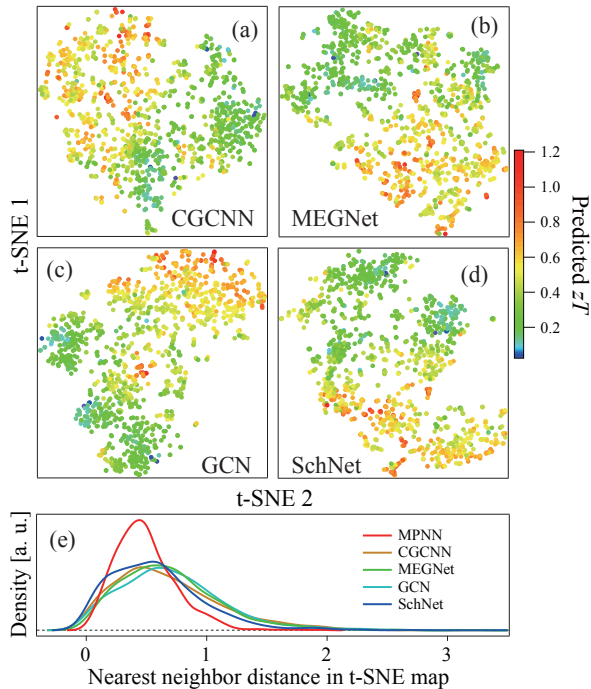


FIG. 5. Comparison of material maps generated by MDL using different graph-based architectures: (a) CGCNN, (b) MEGNet, (c) GCN, and (d) SchNet. (e) The distributions of data points in the maps shown in (a)-(d) are compared by the distribution analysis of NND of each data point by KDE.

Project, while, in this study, we applied a filter based on material stability, band gap, and atomic elements. This screening results in the selection of similar materials, which facilitated feature extraction by machine learning models, leading to material maps with clearer structures.

IV. DISCUSSION

A. Relationship between material property prediction and material map construction

The machine learning model defined in MDL predicts materials properties and generates material maps as part of a continuous process. (Note that this prediction by MDL is different from the prediction of the experimental zT values, described in Ref. [25].) The creation of high-quality material maps indicates the effective extraction of materials features, and thus leads us to anticipate enhanced accuracy in material property predictions. This logic motivate us to evaluate the model performance for the material property prediction by three standard metrics: the coefficient of determination (R^2), mean squared error (MSE), and mean absolute error (MAE) with the data divided into training (80%), testing (15%), and validation (5%) subsets. The evaluation results with the

validation dataset, summarized in Table I, leads that, while the MPNN produces the most structurally interpretable maps, its prediction accuracy ($R^2 = 0.610$) is the lowest among all the models. This unexpected result leads us to conclude that the clear structural organization displayed in the MPNN-derived maps does not necessarily translate to higher predictive performance of the materials properties.

Model	MSE	MAE	R^2
MPNN	0.014594	0.083548	0.610463
CGCNN	0.011580	0.076089	0.690913
MEGNet	0.009895	0.070994	0.735893
GCN	0.007246	0.057658	0.806579
SchNet	0.013064	0.080413	0.651301

TABLE I. Materials property predictions by various graph-based architectures. MSE (Mean Squared Error), MAE (Mean Absolute Error), and R^2 (coefficient of determination) were used as evaluation metrics.

It may be worth noting that MPNN is a graph-based architecture developed relatively early in the field [21] and is characterized by high learnability and versatility. Due to the black-box nature of deep learning-based modeling, it is unclear why the MPNN-generated materials map can capture materials properties so efficiently. Further investigation into the reasons behind these discrepancies could yield valuable insights into how structural interpretability and predictive power might be balanced in future model designs.

B. Improvement of the interpretability of material maps

So far, we mainly discussed the materials maps colored by the predicted zT values, while the computational dataset obtained from the Materials Project encompasses diverse materials data. To improve the interpretability of the obtained maps, we made materials maps colored by the other properties registered in the Materials Projects. Figure 6 shows the maps colored by (a) predicted zT value, (b) energy per atom, (c) number of sites, (d) volume, and (e) number of elements. The following analysis using these rich computational datasets with materials maps provides detailed insights that contribute to a more comprehensive interpretation of the results.

In Figure 6(a), colored by predicted zT , we find the lower values in the bottom left side while high values in the top right and top left sides. Similar trends are found in Figure 6(b), colored by the energy per atom, representing the close relationships between the corresponding parameters. This trend is supported by the high correlation coefficient of 0.66, obtained through the correlation analysis described in SI.

In Figure 2, we find two branches spreading laterally, labeled as BR1 and BR2. The difference of these two branches is identified by seeing the maps colored by the

number of atomic sites and the volume shown in Figures 6(c) and 6(d), respectively. In these figures, we find high and low values for BR1 and BR2, respectively, leading us to attribute the difference of these two branches to the materials complexities. As is clearly represented by the schematics in Figure 2, we find that $\text{Ga}(\text{Ag}_3\text{Se}_2)_3$, representing BR1, exhibits a highly complex structure, whereas Bi_2Te_3 , representing BR2, displays an extremely simple structure.

In Figure 6(e), colored by the number of elements, we find the uniform distribution of the data points. This trend reveals that the structures shown in the map do not represent the complexities in the material composition.

To investigate the distribution of materials in the map, we applied k -means clustering analysis to the map with $k=10$ clusters as shown in Figure 6(f). The label for each cluster was assigned by sorting based on the average of predicted zT values, allowing us to identify regions of high-performance materials. To understand the materials included in each cluster, we counted the number of elements in the compositions of the materials included in each cluster. The elements with less than 10% of the compositional ratio was excluded to account for the elements that make a major contribution to the material properties. The results for each cluster are plotted using the Periodic Trend Plotter (https://github.com/Andrew-S-Rosen/periodic_trends) in Figure 7. In each cluster, we find distinct characteristic distributions of S, Se, and Te atoms. Clusters containing a large number of materials with low zT values (1–7) show a high frequency of S and Se occurrences. On the other hand, clusters containing a large number of materials with high zT values (8–10) exhibit a higher frequency of Te occurrences. In order to find the characteristics of the two branches, labeled as BR1 and BR2 in Figure 2, we compare the elemental distribution for clusters 9 and 10, which are placed at the edge of each branch. We find high similarities between these two plots, such as the high frequencies of Te, Sb, Ti, and Ag atoms. The detailed discussion in terms of the atomic distributions supports our improved understanding of the obtained material maps.

C. Finding proper materials with material maps

Finding optimal materials is extremely important not only in basic research but also in industrial applications, but is always challenging due to the enormous variety of candidate materials. High-throughput screening of materials using computational databases and machine learning is a powerful tool that can suggest promising materials. However, experimental materials researchers frequently face difficulties in developing suggested new materials, due to limited access to raw materials, equipment, facilities, and experimental expertise. Therefore, it is more important to explore promising materials among those that experimental researchers can realistically fabricate.

The material maps developed in this study have great potential to make materials development more efficient because materials with similar structures are likely to be synthesized and characterized using similar methods. For example, researchers working on high-entropy materials, which have significantly complex compositions and structures, require different knowledge and experimental equipment compared to those investigating ordinary materials. The interactive graph, shown in Figure 8, is a powerful tool for targeting specific material properties by referencing aspects such as composition, data names, and other material properties, enabling multifaceted and detailed data exploration. Using Python libraries such as Plotly, interactive graphs can be easily created, and when saved as HTML files, the data can be accessed at any time. The corresponding HTML file is included in the SI. In conclusion, the material maps, which organize materials data based on structural complexity, can assist researchers in screening candidate materials for experimental studies.

D. Prospects for future studies

Data-driven materials development has a potential to revolutionize research and development in various domains, such as inorganic, organic, nano- and pharmaceutical materials. The properties of materials composed of atoms are remarkably diverse, making it challenging to construct a truly universal materials model that applies to all materials.

MDL limits the input data to structural information, and thus the obtained map reflects the structural complexity of materials. By selecting input features, we can tailor the map to meet to specific objectives or explore different aspects of materials behavior. A key avenue for future work involves integrating additional characteristic variables, such as magnetic, chemical, or even topological properties of materials, to create a more comprehensive materials map.

Creation of materials maps requires substantial computational resources, especially for tasks such as dimensionality reduction by the t-SNE architecture and the deep-learning modeling defined in MDL. In this study, we employed the model and the hyperparameters given in MDL due to computational constraints. For wider and better applicability, fine-tuning of the model may be important. Recent advancements in high-performance computing (HPC) and cloud-based GPU/TPU clusters will help mitigate these computational challenges, enabling broader adoption of such methods.

In our study, we integrate computational and experimental data by predicting experimental zT values from compositions [25] by machine learning with experimental dataset of StarryData2 [24]. However, another approach—predicting stable structure from composition—is also conceivable. One should select the method based on the accuracies of the machine learning models,

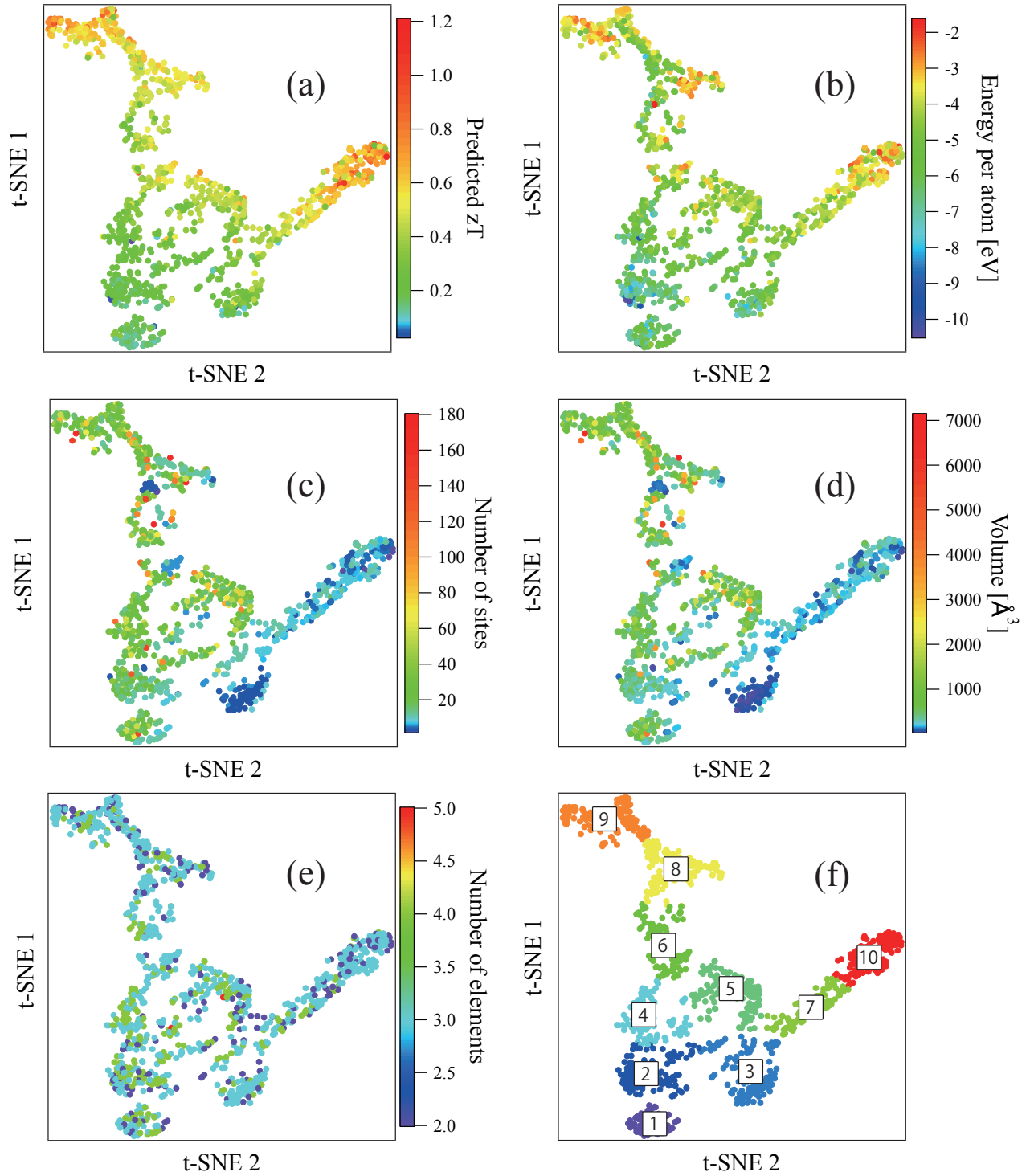


FIG. 6. Material maps generated from the same data used in Figure 2 in the main text, but color-coded by (a) predicted zT , (b) energy per atom, (c) number of sites, (d) volume, and (e) number of elements. (f) Clusters obtained by the k-means clustering with $k=10$.

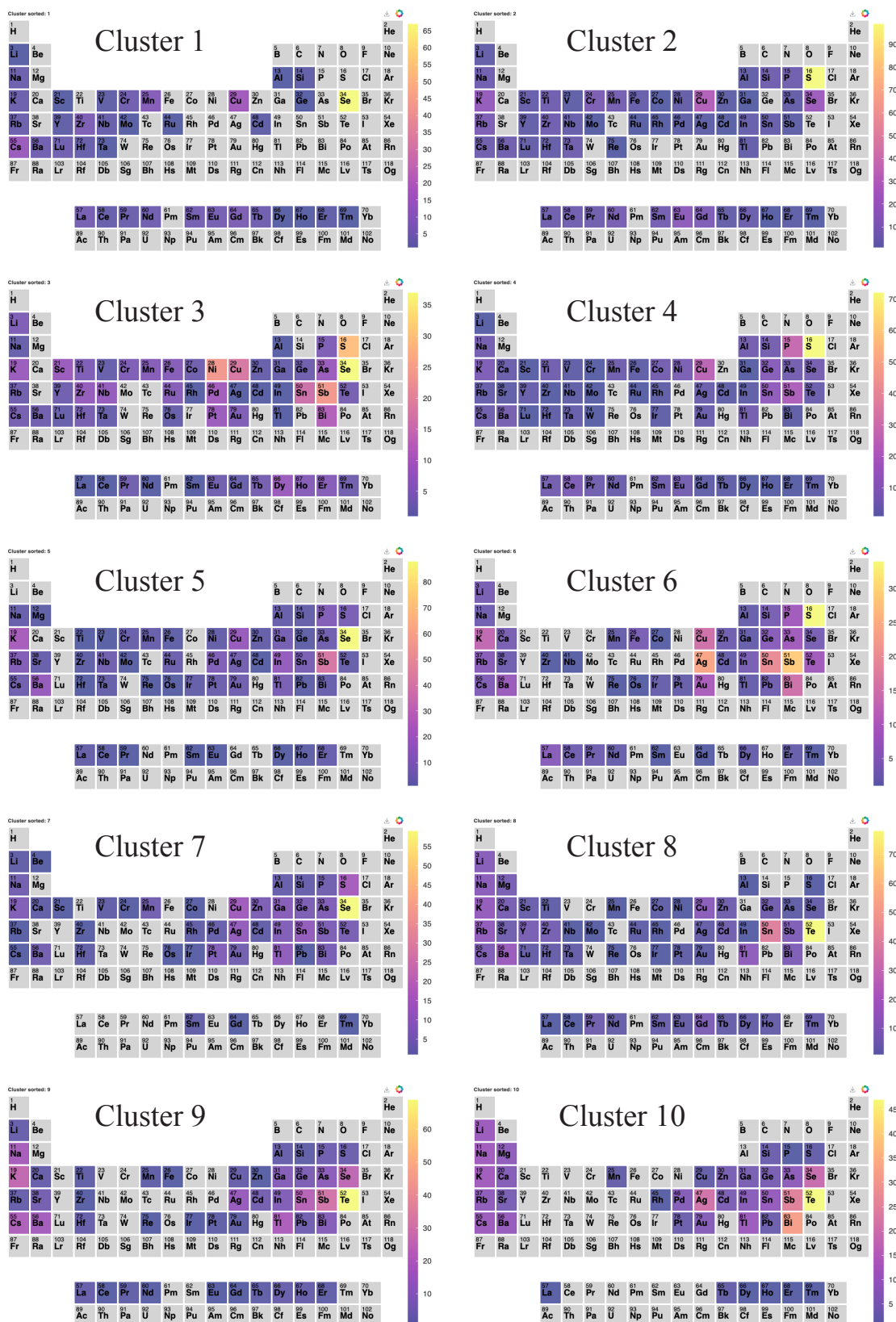


FIG. 7. Analysis results of elements in compositions of included materials in each cluster.

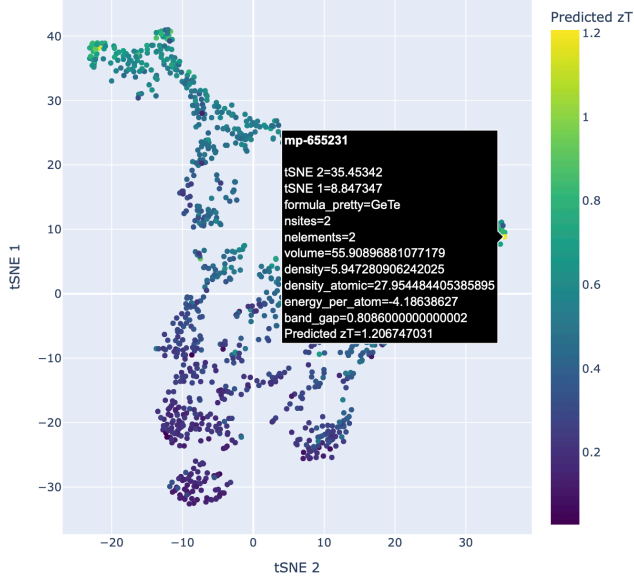


FIG. 8. Interactive graph of materials properties made by Plotly library with the data used in Figure 2.

opting for the approach that achieves higher predictive accuracy. In this study, we employed our approach due to the high prediction accuracy of our model ($R^2 \sim 0.9$), predicting experimental zT values from compositions, and the technical difficulty in the prediction of the stable structure by composition [27]. Moreover, our study focused on the materials containing six selected elements (Sb, Te, Sn, Se, Bi, S), which demonstrated predictive capability for thermoelectric performance through the zT values [25]. Extending this model to encompass a wider range of elements and other physical parameters is left for future studies.

V. CONCLUSION

In this study, we developed and evaluated a novel approach for materials exploration by constructing a materials map that combines graph theory-based model and deep learning. A key feature of our work is the use of materials data from our previous research, which incorporated experimentally predicted values of material properties (zT) along with structural information. The materials maps, generated using the MatDeepLearn (MDL) framework, were evaluated through distribution analysis of nearest-neighbor distances between data points by kernel density estimation. Results showed that among the graph theory-based models supported by MDL, the Message Passing Neural Network (MPNN) provided the most efficient structuring of material properties. Additionally, a systematic evaluation controlled training by the graph convolution layers of MDL demonstrated their significant contribution to the organization of the materials map.

VI. ACKNOWLEDGMENTS

We thank the AIMR ATP project in Tohoku University and Prof. Yong P. Chen’s group for computational support.

VII. SUPPLEMENTAL INFORMATION

A. Data Preparation and Machine Learning

1. Cleaning of zT Data in StarryData2

We use the datasets obtained from the StarryData2 (SD2), an open database for experimental material properties. The initial dataset from SD2 contained various sources of noise and errors, including those from original papers, data mining processes, inadvertent inclusion of calculation data, and extreme experimental conditions. To ensure data quality, we implemented a rigorous cleaning process:

- Removed compositions with typographical errors
- Excluded entries with titles containing keywords indicative of calculations
- Filtered out zT values less than 0 or greater than 3.1
- Omitted studies published before the year 2000

After this cleaning process, 8,541 compositions were selected from SD2.

2. Machine Learning Modeling of Experimental Data

For feature extraction, we utilized Python libraries from matminer, specifically the `elementproperty.from_preset(maggpie)` function. The machine learning model was developed using the following approach:

- Algorithm: Gradient Boosting Decision Tree
- Validation: 10-fold cross-validation
- Data split: 80% training, 20% testing

This process resulted in a machine learning model with an R^2 value of 0.85. Additional data cleaning, which exclude the data showing poor prediction accuracy, again improve the model, reading to $R_2 = 0.90$. Through the composition analysis of the selected materials, we selected Sb, Te, Sn, Se, Bi, and S as key elements for further investigation.

3. Machine Learning Modeling of Calculation Data

To expand our analysis to computational data, we applied our experimental data-trained model to materials from the Materials Project database:

- Selected compositions containing Sb, Te, Sn, Se, Bi, and S

- Filtered for band gap energy above 1.0 eV

- Further filtered for energy hull above 0 eV

As a result, 1,114 compositions were selected. By applying our experimental zT prediction model to this refined set of computational data, we were able to predict experimental zT values for these materials. This approach led to the identification of GeTe_5As_2 and $\text{Ge}_3(\text{Te}_3\text{As})_2$ as potentially high- zT materials.

B. Correlation analysis of parameters

The correlation between the predicted zT values and the parameters stored in the computational datasets (Materials Project) is analyzed using the `.corr()` function in the pandas framework for Python. The correlation coefficient r is defined by

$$r = \frac{\sum_{i=1}^n (x_i - \bar{x})(y_i - \bar{y})}{\sqrt{\sum_{i=1}^n (x_i - \bar{x})^2} \sqrt{\sum_{i=1}^n (y_i - \bar{y})^2}}, \quad (1a)$$

, where

$$\bar{x} = \frac{1}{n} \sum_{i=1}^n x_i, \quad (1b)$$

$$\bar{y} = \frac{1}{n} \sum_{i=1}^n y_i. \quad (1c)$$

The example of r calculated between the predicted zT values and the selected properties stored in the Materials Project are summarized in the following.

Parameter name	Correlation coefficient
Energy per atom	0.65664
Volume	0.05841
Density	0.02604
Number of sites	-0.01809
Number of elements	-0.16573

TABLE S1. Correlation coefficient between predicted zT and the parameters stored in the Materials Projects.

C. Dimensionality Reduction for Materials Map Construction

In this study, we generate material maps by dimensional reduction using the t-SNE algorithm [9], which is implemented using the scikit-learn framework, as in MDL. The default hyperparameters in MDL, which are a perplexity of 50 and a learning rate of 300, were used for the dimensional reduction by t-SNE.

D. Hardware and Software Environment

Calculations for deep learning-based modeling in this study were performed on a workstation equipped with three NVIDIA RTX 3090 GPUs, 128 GB RAM, and an Intel Core i9-10900X CPU @ 3.70GHz. The software used included Python 3.10, TensorFlow 2.10, and the MDL framework.

[1] K. Rajan, *Mater. Today (Kidlington)* **8**, 38 (2005).
 [2] K. Rajan, *Annu. Rev. Mater. Res.* **45**, 153 (2015).
 [3] A. Agrawal and A. Choudhary, *APL Mater.* **4**, 053208 (2016).
 [4] G. R. Schleder, A. C. M. Padilha, C. M. Acosta, M. Costa, and A. Fazzio, *JPhys Mater.* **2**, 032001 (2019).
 [5] J. M. Rickman, T. Lookman, and S. V. Kalinin, *Acta Mater.* **168**, 473 (2019).

[6] A. Jain, S. P. Ong, G. Hautier, W. Chen, W. D. Richards, S. Dacek, S. Cholia, D. Gunter, D. Skinner, G. Ceder, and K. A. Persson, *APL Mater.* **1**, 011002 (2013).
 [7] S. Curtarolo, W. Setyawan, G. L. W. Hart, M. Jahnatek, R. V. Chepulskii, R. H. Taylor, S. Wang, J. Xue, K. Yang, O. Levy, M. J. Mehl, H. T. Stokes, D. O. Demchenko, and D. Morgan, *Comput. Mater. Sci.* **58**, 218 (2012).

- [8] V. Fung, J. Zhang, E. Juarez, and B. G. Sumpter, *Npj Comput. Mater.* **7**, 84 (2021).
- [9] L. van der Maaten and G. Hinton, *Journal of Machine Learning Research* **9**, 2579 (2008).
- [10] G. C. Linderman, M. Rachh, J. G. Hoskins, S. Steinerberger, and Y. Kluger, *Nat. Methods* **16**, 243 (2019).
- [11] D. Kobak and P. Berens, *Nat. Commun.* **10**, 5416 (2019).
- [12] Q. Li, R. Dong, N. Fu, S. S. Omee, L. Wei, and J. Hu, *J. Chem. Inf. Model.* **63**, 3814 (2023).
- [13] C. Liang, Y. Rouzhahong, C. Ye, C. Li, B. Wang, and H. Li, *Nat. Commun.* **14**, 5198 (2023).
- [14] Z. Wang, A. Chen, K. Tao, J. Cai, Y. Han, J. Gao, S. Ye, S. Wang, I. Ali, and J. Li, *Npj Comput. Mater.* **9**, 130 (2023).
- [15] S. S. Omee, S.-Y. Louis, N. Fu, L. Wei, S. Dey, R. Dong, Q. Li, and J. Hu, *Patterns (N. Y.)* **3**, 100491 (2022).
- [16] T. Ehiro, *Mol. Inform.* **42**, e2300061 (2023).
- [17] L. McInnes, J. Healy, and J. Melville, arXiv:1802.03426 (2018).
- [18] A. S. Rosen, S. M. Iyer, D. Ray, Z. Yao, A. Aspuru-Guzik, L. Gagliardi, J. M. Notestein, and R. Q. Snurr, *Matter* **4**, 1578 (2021).
- [19] H. Park, R. Zhu, E. A. Huerta, S. Chaudhuri, E. Tajkhorshid, and D. Cooper, *Mach. Learn. Sci. Technol.* **4**, 025036 (2023).
- [20] T. Xie and J. C. Grossman, *Phys. Rev. Lett.* **120**, 145301 (2018).
- [21] J. Gilmer, S. S. Schoenholz, P. F. Riley, O. Vinyals, and G. E. Dahl, arXiv:1704.01212 (2017).
- [22] C. Chen, W. Ye, Y. Zuo, C. Zheng, and S. P. Ong, *Chem. Mater.* **31**, 3564 (2019).
- [23] K. T. Schütt, P.-J. Kindermans, H. E. Sauceda, S. Chmiela, A. Tkatchenko, and K.-R. Müller, in *Proceedings of the 31st International Conference on Neural Information Processing Systems, NIPS'17* (Curran Associates Inc., Red Hook, NY, USA, 2017) pp. 992–1002.
- [24] Y. Katsura, M. Kumagai, T. Kodani, M. Kaneshige, Y. Ando, S. Gunji, Y. Imai, H. Ouchi, K. Tobita, K. Kimura, and K. Tsuda, *Sci. Technol. Adv. Mater.* **20**, 511 (2019).
- [25] X. Jia, A. Aziz, Y. Hashimoto, and H. Li, *Sci. China Mater.* **67**, 1173–1182 (2024).
- [26] E. Parzen, *Ann. Math. Stat.* **33**, 1065 (1962).
- [27] V. V. Gusev, D. Adamson, A. Deligkas, D. Antypov, C. M. Collins, P. Krysta, I. Potapov, G. R. Darling, M. S. Dyer, P. Spirakis, and M. J. Rosseinsky, *Nature* **619**, 68 (2023).